Theory of the Temporal Response of a Simple Multiquantum-Well Avalanche Photodiode

KEVIN F. BRENNAN, MEMBER, IEEE, YANG WANG, MALVIN C. TEICH, SENIOR MEMBER, IEEE, BAHAA E. A. SALEH, SENIOR MEMBER, IEEE, AND TOOFAN KHORSANDI, STUDENT MEMBER, IEEE

Abstract—**We present numerical and analytically based calculations of the impulse response function of a simple GaAs/AlGaAs multiquantum-well avalanche photodiode. The numerical approach involves the direct simulation of the electron and hole transport in the device. An iterative approach is used in that the parent electron distribution is first simulated yielding the velocity profile as a function of position, transit-time distribution of the parent and daughter electrons, and the daughter-hole distribution. The daughter-hole distribution is subsequently simulated using the time of birth and spatial location of each secondary hole as initial conditions. The calculation continues iteratively in this fashion yielding a picture of the time evolution of the impulse response function. The analytical calculation is based on the use of a marked filtered Bernoulli branching process. Each event of this process contributes electron and hole component currents appropriate to the times and positions of the particle births. Both analytical and simulation results are presented for single-carrier-initiated single-carrier-multiplication (SCISCM) devices. The similarities and differences in the outcomes of the two approaches are instructive. Only simulation results are presented for devices in which secondary hole-initiated ionization occurs.**

I. INTRODUCTION

THE performance of a lightwave communications system is judged by its ability to transmit and receive well-defined optical pulses at a high rate with a low incidence of error. Receiver performance is determined by measures such as the bit error rate (which is dependent on intersymbol interference) and the bandwidth. Presently, optical communications system performance is primarily limited by detector or receiver noise.

Avalanche photodiodes (APD's) are widely used as the detector elements in high-speed digital lightwave communications networks owing to their relatively large gain-bandwidth product at acceptable noise levels. The gain, and excess noise factor of an avalanching device, depend predominantly on the ratio of the electron to hole ionization coefficients [1]–[3]. However, the maximum bit detection rate, as well as the probability of error, require a more detailed description of the carrier currents.

APD's operate by converting incident absorbed photons into cascades of electron–hole pairs [4], [5]. Specifically, an absorbed photon produces an initial electron–hole pair (parent carriers) within the front-illuminated p^+ contact. Due to the action of a reverse-bias field, the hole is immediately swept out of the contact while the electron is accelerated through the depletion region. Under high reverse bias, the electron, on average, attains sufficiently high energy for impact ionization giving rise to a secondary electron–hole pair. The initial and secondary carriers resume their flight through the device during which additional electron–hole pairs are produced. In this way, a cascade of secondary carriers is generated by each incident photogenerated electron.

The multiplication process introduces noise due to fluctuations in the number of secondary carriers created per detected photon. This noise, which arises in addition to the usual shot and thermal noises present in an electronic device (hence its name, excess noise), is minimized under single-carrier-initiated single-carrier multiplication (SCISCM) conditions [1]–[3], [6]. The bandwidth, which is the inverse of the time of response of the detector, also achieves its optimal (largest) value under SCISCM conditions. Therefore, for high-speed and low-noise operation, an APD must be operated such that only one carrier species ionizes.

APD's that are made from most III-V semiconducting material systems (which are sensitive to radiation most useful in lightwave communications) cannot simultaneously provide high gain, low noise, and large bandwidth owing to the nearly equal electron and hole ionization coefficients. Thus, further engineering of the material, i.e., the use of superlattices or multiquantum-well structures, is desirable. Chin *et al.* [7] first suggested a means of artificially enhancing the electron-to-hole ionization rates ratio, and consequently improving the gain, noise, and bandwidth performance of the detector, through the use of a multiquantum-well/superlattice structure. Owing to the greater conduction to valence band-edge discontinuity in the GaAs/AlGaAs lattice matched heterostructure system, they predicted that the electron ionization rate would be sizeably greater than the corre-

Manuscript received February 22, 1988; revised April 29, 1988. This work was supported in part (Georgia Tech) by the Polaroid Corporation under Contract B-10-635 and by the National Science Foundation (Columbia University and University of Wisconsin).

K. F. Brennan and Y. Wang are with the School of Electrical Engineering and the Microelectronics Research Center, Georgia Institute of Technology, Atlanta, GA 30332-0250.

M. C. Teich is with the Center for Telecommunications Research, Department of Electrical Engineering, Columbia University, New York, NY 10027 and with the Department of Electrical and Computer Engineering, University of Wisconsin, Madison, WI 53706.

B. E. A. Saleh is with the Department of Electrical and Computer Engineering, University of Wisconsin, Madison, WI 53706.

T. Khorsandi is with the Center for Telecommunications Research, Department of Electrical Engineering, Columbia University, New York, NY 10027.

IEEE Log Number 8822116.

sponding hole ionization rate. Subsequent experimental measurements [8]–[10] and theoretical analyses [11]–[14] have confirmed that the electron ionization rate can be significantly enhanced over both its bulk value and the hole ionization rate within superlattice structures.

Several general methods have been devised that act to artificially enhance the electron-to-hole ionization rates ratio through selective heating of the electron distribution. Among these techniques are the use of heterostructure potential-step discontinuities as in a multiquantum well/superlattice structure [7], [15], [16]; the use of a built-in electric field arising from a fully depleted p-i-n [17]–[19], p-n homojunction [20], or p-n heterojunction [21] in conjunction with a band-edge discontinuity; the use of impact ionization from confined quantum-well states [22]–[24]; the use of resonant tunneling in a superlattice structure [25], [26]; and the use of a separate absorption grading and multiplication layer device (SAGM-APD) [27]. In all of these devices, the electron ionization rate is greatly enhanced over the hole ionization rate and is also made more spatially deterministic than in conventional APD's. This has the additional feature of further lowering the excess noise figure from that possible within a conventional APD [3], [28].

Aside from the gain and excess noise factor, it is important to determine the bandwidth, or equivalently the temporal response of the device, as well as the bit error rate in order to fully characterize the detector as a receiver in digital communications systems [29]. Both the temporal response as well as the bit error rate depend upon a complete statistical description of the electron current. The bit error rate, the ability of the detector to distinguish between a "one" and a "zero," is most dependent upon the tails of the counting distributions, which are generally only weakly reflected in the excess noise factor [30]. It is difficult to analytically determine the bandwidth in the presence of residual secondary hole ionization.

The bandwidth is determined in part by how quickly the current pulse, generated by an incident pulse of photons, decays. If an APD exhibits considerable time dispersion, its ability to handle a high-speed data train is severely compromised. Adjacent pulses "bleed" into one another causing what is known as intersymbol interference [29]. Consequently, the APD will fail to discern separate pulses, which leads to detection errors.

The time reponse of an APD is shortest in the absence of secondary hole ionization; it then depends only upon the combined transit times of the electrons and holes. However, when the secondary holes (those produced from electron-initiated impact ionization events) impact ionize (SCIDCM conditions), the impulse response shows considerable broadening [31]–[33].

We present numerical and analytical calculations of the impulse response function of a simple multiquantum-well superlattice avalanche photodiode (MQW SAPD) made from the GaAs/AlGaAs material system (see Fig. 1). The analytical formulation is based on the use of a Bernoulli branching process [6], [30]. Each event of this process is

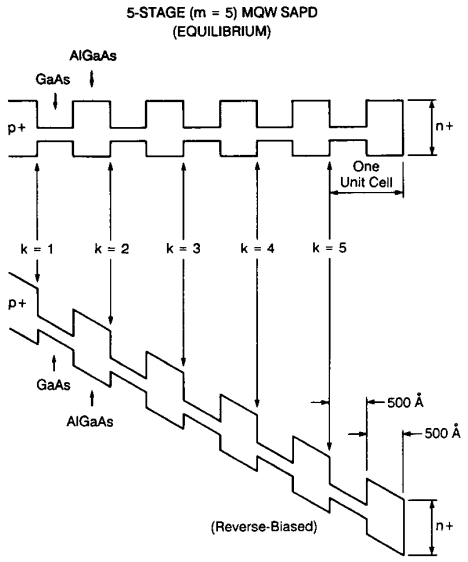

Fig. 1. Energy-band diagram of the multiquantum-well (MQW) superlattice avalanche photodiode (SAPD) under (a) unbiased (equilibrium) and (b) reverse-biased conditions. For the purposes of illustration and calculation, the device consists of m stages ($m = 5$ is shown), each of which comprises a 500-Å layer of GaAs followed by a 500-Å layer of AlGaAs.

marked by simple electron and hole component currents appropriate to the times and positions of the particle births. The analytical approach is similar to that used previously for the staircase superlattice APD [6]. The numerical approach involves the direct simulation of the carrier transport in the device via an ensemble Monte Carlo calculation. From the simulation, both the temporal response as well as the gain fluctuation can be ascertained. The details of the numerical and analytical formulations are presented in Sections II and III, respectively. The calculations for SCISCM conditions are discussed in Section IV, while those for SCIDCM conditions are presented in Section V. Finally, conclusions are drawn in Section VI.

II. Description of the Numerical Calculations

The numerical calculations are based on the direct simulation of the underlying microscopic current processes that dictate the device performance. The calculations are performed using the ensemble Monte Carlo technique, which consists of the simulation of the trajectories of a collection of carriers in the device structure subject to an applied electric field in conjunction with the device potential profile. The carrier histories are traced in both real and k-space including the full details of the conduction and valence band structures and all of the relevant phonon-scattering mechanisms [34]. In this way, the time evolution of a photogenerated pulse of electrons is rigorously determined.

The temporal response of the device is defined as the time course of the current delivered by the device to the external circuit in response to a single photogenerated carrier pair. The total current is the superposition of the electron and hole currents generated in the circuit from within

the semiconductor, which are instantaneously proportional to the carrier velocities. Each initially injected photogenerated electron (parent electron) traverses the entire length of the device and, therefore, delivers a complete charge q to the external circuit. Each secondary electron–hole pair created within the device, from an impact ionization event, also delivers a net charge q to the external circuit. Therefore, each individual electron created within the depletion region of the APD induces only a portion of the total charge q in the external circuit, such that the total charge arising from the motion of the electron and hole taken together is q. Another way of understanding this is to recall that current flow is defined as the passage of a charge through a complete circuit. Within the semiconductor, the total path is partly traversed by the electron and partly by the hole, such that the total distance traveled together is equal to the total device length W. As a simple bookkeeping tool, we define the charge delivered by each electron and hole separately as an effective charge whose total for each electron–hole pair sums to q. The electron and hole effective charges are defined, then, as

$$q_e^* = \int i_e(t)\,dt$$
$$q_h^* = \int i_h(t)\,dt \qquad (1)$$

where $q = q_e^* + q_h^*$, and i_e and i_h are the electron and hole currents, respectively. The total charge delivered is then

$$q = \int i_e(t)\,dt + \int i_h(t)\,dt. \qquad (2)$$

The contribution to the circuit current $i_e(t)$ for an individual carrier traversing a multiquantum-well superlattice avalanche photodiode depends on the carrier velocity in the device $v_e(t)$, in accordance with the relation $i_e(t) = (q/w)v_e(t)$, where q is the electronic charge and w is the length of the device. This relation is obtained by applying the well-known general result $j(t) = \rho v(t)$ (where $j(t)$ is the current density and ρ is the charge density) to a volume comprised of cross-sectional area A and length w. The time course of the overall current pulse $i(t) \equiv i_T(t)$ generated in the external circuit by an avalanche of carriers built up from a single photogenerated carrier is simply obtained by superimposing the time-dependent velocities of the initial carrier, and those of the daughter electrons and holes created at the AlGaAs–GaAs conduction-band interfaces, as indicated below. The effective charge delivered by the electron to the circuit is, therefore, the ratio of the integral of the electron instantaneous velocity over time to the sum of the integrals of the electron and hole instantaneous velocities over time multiplied by the total charge q, i.e.,

$$q_e^* = q \int v_e(t)\,dt \Big/ \left[\int v_e(t)\,dt + \int v_h(t)\,dt \right]. \qquad (3)$$

Notice, however, that the denominator of (3) is simply equal to the total length of the device w. Therefore, the total current delivered to the external circuit becomes

$$i_T(t) = \sum \left(i_e(t) + i_h(t)\right)$$
$$i_T(t) = (q/w) \sum v_e(t) + (q/w) \sum v_h(t) \qquad (4)$$

where the sums are taken over *all* of the carriers present, parents and daughters. Therefore, the total current is found from the sum, over the total number of carriers of the instantaneous carrier velocity at that time multiplied by the ratio of the electron charge q to the total device length w.

The actual simulation involves an iterative approach. First, a deterministic number of photogenerated electrons are launched and their motion through the device is tracked. When an impact ionization event occurs, the time and spatial location of the secondary electron–hole pair is recorded and the daughter electron is added to the simulation. This continues until all of the initial parent electrons, and all of the secondary electrons born of them, are collected at the n^+ contact. The electron current at a fixed time t is given by the sum of the instantaneous electron velocities calculated from the gradient of the $E(k)$ relation. This current response is called the electron current in the first iteration.

The hole transit histories are next simulated, using as the initial condition the holes born in the first iteration for the electrons. The random number of holes are launched in accordance with their spatial locations determined in the first iteration, and their time of flight is equal to the sum of their transit time and the time delay prior to their birth. The instantaneous hole current is found in a way similar to that for the electrons. Again, the simulation ends after the initial holes, and all of the secondary holes born from hole-initiated impact ionization events, are collected at the p^+ contact. The secondary electrons born from these events are tracked in the second electron iteration, using as initial conditions the spatial location of the electron births as well as the time delay in their production. The total current is calculated after the electron and hole first iterations from (4). In general then, successive iterations are based on the birth locations and times derived from the former iteration, which are used as the input of the current iteration. The birth locations and times of the daughter carriers produced in the current iteration are recorded and used in the next iteration. It is important to note that the behavior of each electron and hole, once born, is statistically independent of the others. Therefore, the electron and hole currents can be calculated as described above.

We present results for three complete iterations of the electron and hole transport in a simple GaAs/AlGaAs multiquantum-well APD, consisting of 500-Å barriers and wells. The devices are assumed to have five full stages ($m = 5$). We then calculate the standard deviation of the impulse response function that results from both randomness in the gain and in the birth times. The standard deviation of the impulse response function is obtained by

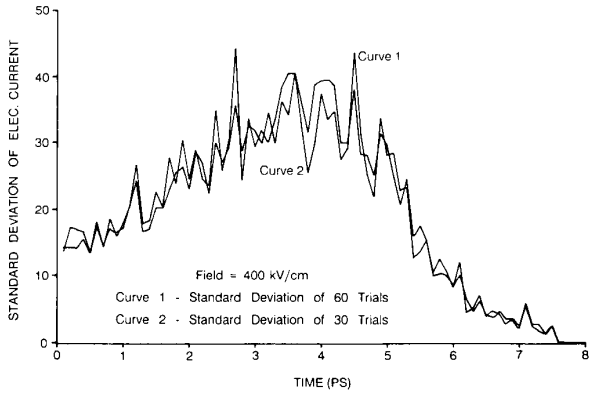

Fig. 2. Standard deviation of the electron current after 60 (curve 1) and 30 (curve 2) trials determined from use of the Monte Carlo simulation.

simulating numerous subensembles of carriers. The mean response and standard deviation of this set of subensembles is then obtained. The number of trials is determined by examining the rate of convergence of the calculation. As an example, the standard deviation of the electron current is shown in Fig. 2 after 30 and 60 trials. Although the convergence is evident, we use 60 trials in all of our calculations.

Because of computer time limitations, results are presented only for the standard deviation of the electron current. In order to obtain different histories, the random-number seed is altered after each trial.

III. Description of the Analytical Model

The simulation studies described in Section II have been used to provide the electron velocity profile, as a function of position, for a single electron traversing the entire depletion region of the MQW SAPD device. Presently we lack the full details of the AlGaAs conduction band. In its place, we use a modified version of the pseudopotential generated GaAs conduction band in the sense that the bandgap and threshold energy are adjusted accordingly. The lack of the current low-energy details of the AlGaAs conduction band has little effect on the impact ionization rate, but can significantly effect the calculation of the velocities. Nevertheless, the calculations presented here give a reasonable estimate of the velocity profile. A more refined calculation is in progress. This velocity profile is shown in Fig. 3(a) for a five-stage device ($m = 5$) consisting of 500-Å alternating layers of GaAs and AlGaAs. The analogous velocity profile for a single hole, transiting backward through four stages of the depletion region of the device, is illustrated in Fig. 4(a). The electron velocities are on the average larger in the small bandgap material than in the large bandgap material. This is in accord with expectations from a simple model in which momentum increases with increasing energy. The hole velocities have just about the same average value in both materials. For both electrons and holes, there are substantial peaks in the carrier velocity at both the GaAs/AlGaAs and the AlGaAs/GaAs band-edge discontinuities.

A. Underlying Physical Basis

These position-dependent electron and hole velocity profiles are most readily idealized by using the average carrier velocities in the two materials as shown in Figs. 3(b) and 4(b), respectively. The mean electron velocities in the two materials are then $v_e(\text{GaAs}) = 1.0 \times 10^7$ cm/s and $v_e(\text{AlGaAs}) = 9.10 \times 10^6$ cm/s, and the mean hole velocities are taken to be the same, 7.30×10^6 cm/s. Comparison of Figs. 3(a) and (b) with Figs. 4(a) and (b), respectively, shows that the use of a simple two-velocity model for the analytical calculations is far from ideal, but it is of interest to see how well this simple model will do in predicting the impulse response function.

Calculation of the MQW SAPD circuit current requires the *time*-dependent velocity profiles of the carriers, rather than the *position*-dependent velocity profiles. This conversion is readily effected for the two-velocity model, and is illustrated in Fig. 5. The current contribution $a_k^{(m)}(t)$ for an electron born (or injected) at the kth unit cell (see Fig. 1) is presented in Fig. 5(a). The mean electron transit times in the two materials, $\tau_e(\text{GaAs})$ and $\tau_e(\text{AlGaAs})$, are indicated. These transit times are obtained from the relationship $\tau_{e,h}(\text{GaAs, AlGaAs}) = d/v_{e,h}(\text{GaAs, AlGaAs})$, where d is the layer width (500 Å). The sketch shows $\tau_e(\text{AlGaAs}) > \tau_e(\text{GaAs})$. This is a result of the fact that $v_e(\text{AlGaAs}) < v_e(\text{GaAs})$, i.e., that the electron spends more time in the AlGaAs on average. The analogous current contribution $b_k^{(m)}(t)$ for a hole born at the kth unit cell is shown in Fig. 5(b). Here, $\tau_h(\text{AlGaAs}) \sim \tau_h(\text{GaAs})$, because the hole spends about the same time in the AlGaAs as in the GaAs on average. More generally, T_h will differ in the two materials as shown in the sketch. T_e and T_h are defined as the mean electron and hole transit times across one unit cell of the structure, respectively, i.e.,

$$T_e = \tau_e(\text{GaAs}) + \tau_e(\text{AlGaAs}) \tag{5a}$$

$$T_h = \tau_h(\text{GaAs}) + \tau_h(\text{AlGaAs}). \tag{5b}$$

The mean current is q/mT_e and q/mT_h for the electron and hole, respectively. The total charge contributed to the MQW SAPD circuit from an electron–hole pair born at an arbitrary location within the depletion region ($1 \leq k \leq m$) is q. This may be easily verified by integrating the two current pulses shown in Fig. 5 and then summing them.

An examination of Fig. 1(b) demonstrates that the initially injected electron drifts the entire length of the device before arriving at the n^+ contact. Assuming short-circuit device conditions, this produces a current pulse in the circuit beginning at $t = 0$ and extending to $t = 5T_e$, with mean value $q/5T_e$, as shown in Fig. 5(a) with $k = 1$. The total charge delivered to the circuit by this electron is q. The initial hole does not contribute to the current because it is immediately swept out and traverses no distance.

If one of the initial electrons creates an electron–hole pair at the second AlGaAs–GaAs interface, for example,

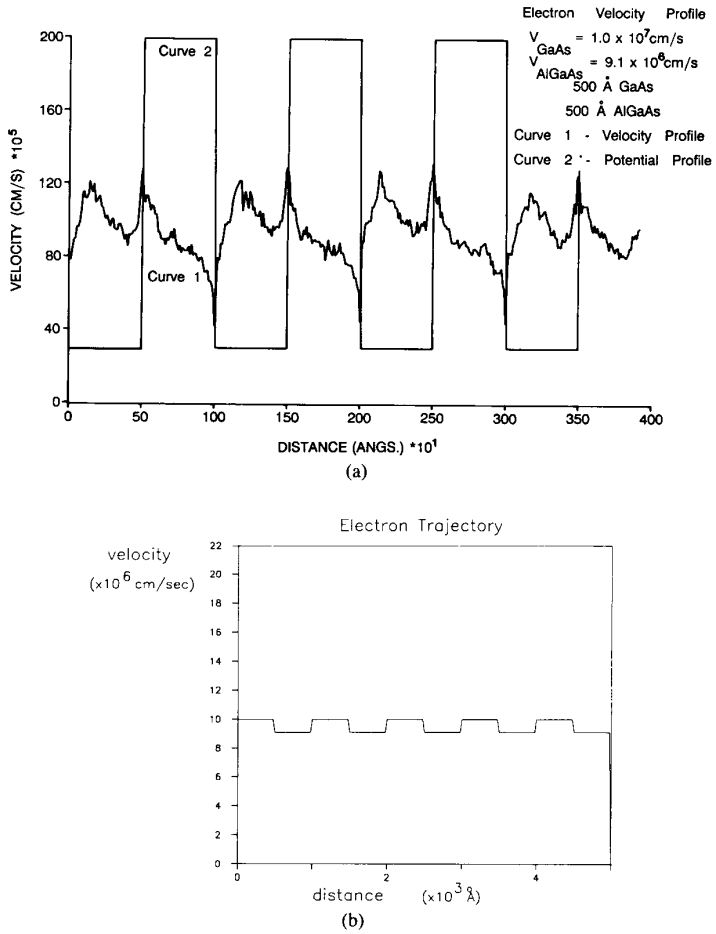

Fig. 3. Electron velocity profile, as a function of position, for a single electron traversing the entire depletion region of the MQW SAPD device. The velocity profile obtained from the multiparticle Monte Carlo simulation is shown in (a) for a five-stage device ($m = 5$) consisting of 500-Å alternating layers of GaAs and AlGaAs. The idealized profile shown in (b), with mean electron velocities in the two materials given by $v_e(\text{GaAs}) = 1.0 \times 10^7$ cm/s and $v_e(\text{AlGaAs}) = 9.1 \times 10^6$ cm/s, is used for the analytical calculations.

where $k = 2$ (this happens with probability P), the daughter electron will give rise to a current pulse in the circuit that is delayed by T_e and of shorter duration than the primary pulse (i.e., of duration $(m-1)T_e$ rather than mT_e), but of the same magnitude (q/mT_e). On the other hand, the conjugate hole travels backward, traversing one unit cell before reaching the contact. It, therefore, contributes a current pulse delayed by T_e, with duration T_h, and mean magnitude q/mT_h.

B. Theory

The flow diagram for the current pulse generated in the circuit of a general m-stage SAPD, by a single photogenerated carrier undergoing random Bernoulli multiplication, is presented in Fig. 6. The single photogenerated carrier is represented by the input $\delta(t)$. The current pulses generated by individual electrons and holes created at the kth unit cell are designated $a_k^{(m)}(t)$ and $b_k^{(m)}(t)$, respectively, as illustrated in Fig. 5. The current pulse arising from the carrier born at the first unit cell ($k = 1$) is identical to that created by the initial photogenerated carrier since they both traverse all m stages of the device. Thus

$$a_0^{(m)}(t) = a_1^{(m)}(t). \tag{6}$$

As indicated above, holes at the p^+ contact will contribute no current so that

$$b_1^{(m)}(t) = 0. \tag{7}$$

The quantities $z_1, z_2, \cdots, z_k, \cdots, z_m$ are independent identically distributed Bernoulli random variables satisfying $Pr[z = 0] = 1 - P$ and $Pr[z = 1] = P$. The electron current pulses $i_e^{(m)}(t)$ and the hole current pulse $i_h^{(m)}(t)$ are sums of the constituent a_k's and b_k's, respectively, weighted by the appropriate Bernoulli random variables representing their likelihoods of contribution. The total current pulse $i_T^{(m)}(t)$ is, in turn, a superposition of the electron and hole currents. Since the total current pulse represents the response to a single primary event, it is equivalently designated as $i(t)$ or as the single-injected-carrier impulse response function $h^{(m)}(t)$, i.e.,

$$i_T^{(m)}(t) \equiv h^{(m)}(t) \equiv i(t). \tag{8}$$

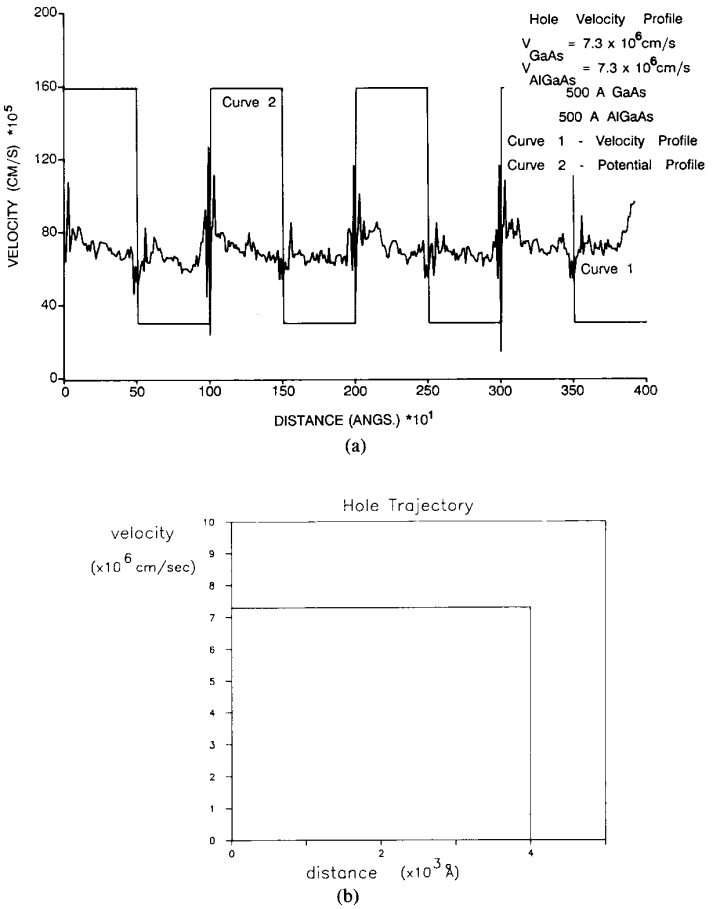

Fig. 4. Hole velocity profile, as a function of position, for a single hole transiting backward through four stages of the depletion region of the device. The velocity profile obtained from the multiparticle Monte Carlo simulation is shown in (a) for an $m = 5$ device consisting of 500-Å alternating layers of GaAs and AlGaAs. The idealized profile shown in (b), with mean hole velocities in the two materials both given by 7.0×10^6 cm/s, is used for the analytical calculations.

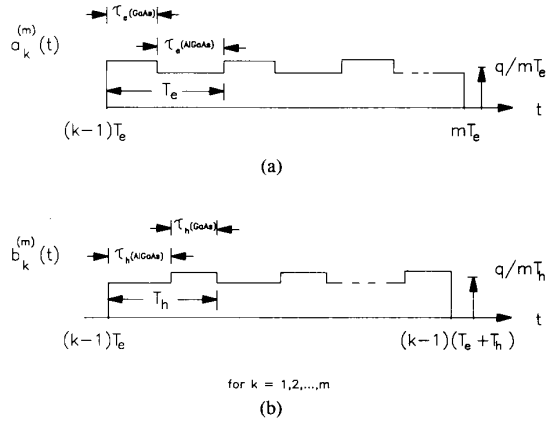

Fig. 5. Current contributions for (a) an individual electron and (b) an individual hole born (or injected) at the kth unit cell of an m-stage MQW SAPD. These current contributions are proportional to the time-dependent velocity profiles of the carriers. The electron and hole transit times τ in the two materials are shown, as are the mean electron and hole transit times across one unit cell of the structure, denoted T_e and T_h, respectively. The mean current is q/mT_e and q/mT_h for the electron and the hole, respectively. The total charge contributed to the MQW SAPD circuit from an electron–hole pair born at an arbitrary location within the depletion region ($1 \leq k \leq m$) is q.

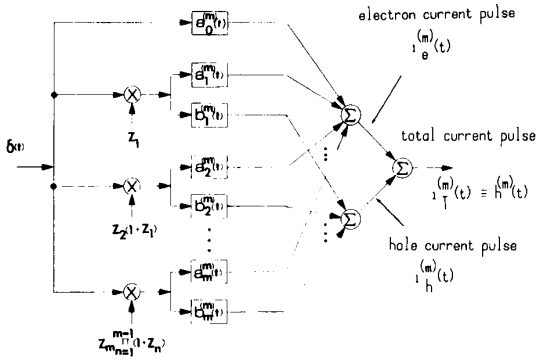

Fig. 6. Flow diagram detailing contributions to the single-photon impulse response function $h^{(m)}(t)$ for the m-stage SAPD with time dynamics. The input $\delta(t)$ represents the presence of a single photogenerated carrier. the a_k's and b_k's are component electron and hole currents, respectively, whereas the z_k's are Bernoulli random variables. The total current is equivalently designated as $i_T^{(m)}(t)$ or $h^{(m)}(t)$ or simply $i(t)$.

Although the diagram presented in Fig. 6 is the same as that used previously for the staircase SAPD [6, Fig. 6(a)], the a_k's and b_k's differ in the two structures. This is because the velocities of the electrons and holes in the

graded regions of the staircase SAPD are well modeled by constant values whereas the MQW SAPD requires a more complex velocity model for the electrons.

The flow diagram of Fig. 6 is easily translated into a mathematical expression for the (random) total current $i(t)$ [6, eq. (13)]

$$i(t) = a_0^{(m)}(t) + \sum_{k=1}^{m} z_k\left[a_k^{(m)}(t) + b_k^{(m)}(t)\right] \cdot \prod_{n=1}^{k-1}(1 + z_n), \qquad m \geq 1. \tag{9}$$

The functions $a_k^{(m)}(t)$ and $b_k^{(m)}(t)$ are displayed in Fig. 5.

The mean of (9), therefore, is written as

$$\langle i(t)\rangle = \langle a_0^{(m)}(t)\rangle + P\sum_{k=1}^{m}(1+P)^{k-1} \cdot \left[\langle a_k^{(m)}(t)\rangle + \langle b_k^{(m)}(t)\rangle\right] \tag{10}$$

representing the mean circuit-current impulse response function induced by a single injected carrier. Expressions for the mean-square current $\langle [i(t)]^2 \rangle$ and the autocorrelation function of the current $R^{(m)}(t_1, t_2)$ are omitted because of their length.

C. Random Transit Time

A more accurate model would ascribe randomness to the four velocities (and, therefore, to the four transit times) of the carriers, and would also permit them to assume values that differ from stage to stage. We have obtained an approximate probability density function for the electron transit time across an MQW SAPD device structure consisting of five unit cells for a field of 400 kV/cm using our simulation analysis. The result is illustrated in Fig. 7; it turns out to have a shape that is rather Gaussian-like with a standard deviation σ_e that is about 14 percent of the mean electron transit time $\langle \tau_e \rangle$, i.e., the coefficient of variation of the transit time is given by

$$\sigma_e/\langle \tau_e \rangle \approx 0.14. \tag{11}$$

Although the impulse response function can be obtained for an analytical model that incorporates random transit times [6], the expression is complex and difficult to deal with. The idealization that we have used here, which invokes three constant velocities, turns out to be acceptable as will become apparent when we compare the analytical and simulation results for the impulse response function in the next section.

IV. Comparison of Impulse Response Functions Obtained from Simulation and Analytical Studies

It is of interest to compare the MQW SAPD impulse response functions obtained from simulation and from analytical modeling. This is useful in establishing the validity of, and ascertaining the roles played by, various elements in both models. The examples provided are for a five-stage ($m = 5$) MQW SAPD structure with alternating layers of GaAs and AlGaAs, each of 500-Å thickness, operated at a field of 400 kV/cm. Hole-initiated impact ionization is assumed to be absent in both cases ($Q = 0$).

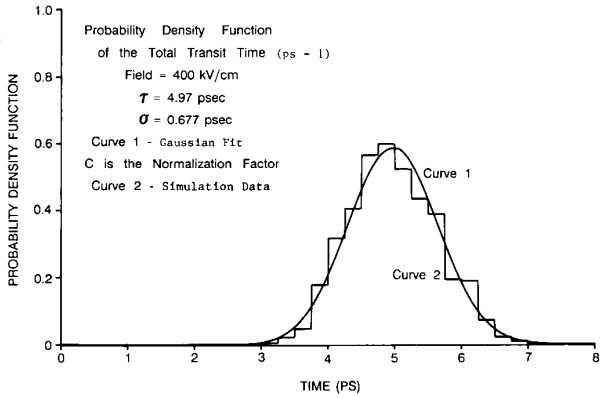

Fig. 7. Simulation result for the approximate probability density function for electron transit time across five unit cells of the MQW SAPD, with a field of 400 kV/cm. The shape of the distribution plotted in curve 2 resembles the Gaussian distribution plotted in curve 1, where $\sigma_e = 0.677$ and $\langle \tau_e \rangle$ is equal to the mean of the total transit time, 4.97 ps.

The impulse response functions obtained from the simulation and from the analytical model are illustrated in Fig. 8(a) and (b), respectively. The electron impact ionization probability P used in the calculations was chosen to be 0.338 to render the gain identical in both cases. The ordinate units for the simulation result are proportional to the total number of carriers used for the simulation whereas those for the analytical result assume a single initial carrier. The abscissa units for the simulation results are directly in picoseconds whereas those for the analytical results are in units of T_e, which is the electron transit time across one unit cell of the device. Since the width of the unit cell is $2d = 1000$ Å, and the mean electron velocity is $\approx 10^7$ cm/s, $T_e \approx 1$ ps, and the abscissas are essentially identical.

The general similiarity of the impulse response functions presented in Fig. 8(a) and (b) is apparent, indicating the general capabilities of both models for predicting the impulse response function. In particular, both curves initially exhibit a rising region with undulations. The general increase is associated with the multiplication process whereas the undulations reflect the velocity modulation as the electrons alternately traverse GaAs and AlGaAs. Both curves peak at about $4T_e$; this is, in fact, the time at which the last impact ionization occurs in this five-stage device. Finally, beyond $4T_e$, both curves decay and exhibit a rather flat tail that reflects the backward transit of the nonionizing holes through the depletion region of the device.

Several subtle distinctions between the curves are worthy of mention. These are interesting in that they reflect differences in the two approaches. The analytical impulse response function is generally less smooth than the simulation function and it exhibits a shorter tail. Both of these characteristics can be attributed to the assumption of constant transit time (velocity) for each carrier in each material in the analytical model. As indicated earlier, transit-

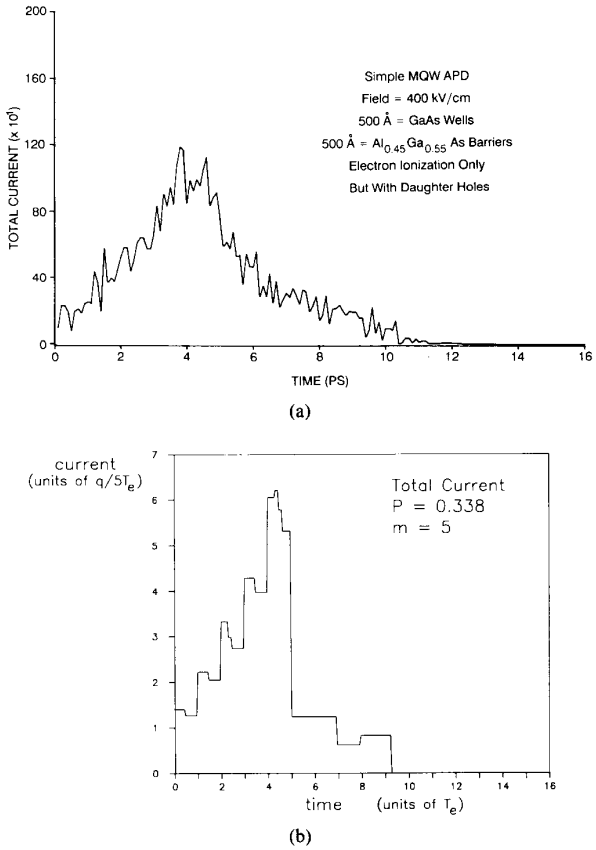

Fig. 8. Comparison of impulse response functions obtained from (a) simulation and (b) from analytical modeling for a five-stage MQW SAPD structure with alternating layers of GaAs and AlGaAs, of 500-Å thickness each, operated at a field of 400 kV/cm. Hole-initiated impact ionization is assumed to be absent in both cases ($Q = 0$). The ordinates are arbitrary but the abscissas have essentially identical units. Although the general similarity of the impulse response functions is apparent, subtle distinctions reflect differences in the two approaches.

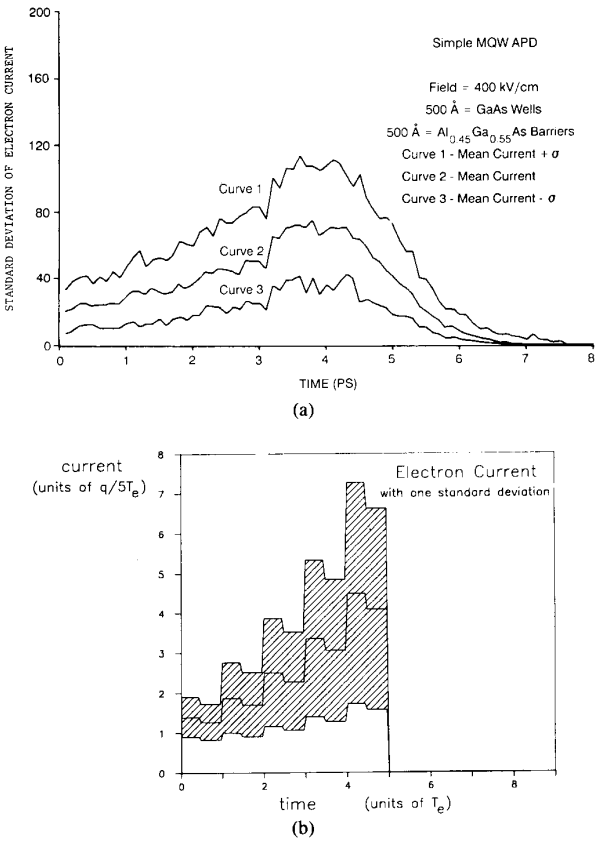

Fig. 9. Electron-current contributions to the impulse response function, together with their one-standard-deviation (1-SD) limits, for (a) simulation and (b) analytical calculations. Uncertainty can arise from both gain randomness and transit-time randomness, as reflected in (a). Only gain randomness is permitted to occur in (this version of) the deterministic transit-time analytical model.

time dispersion is embodied in the simulation model but not in (this version of) the analytical model. We have previously shown that the effect of transit-time dispersion is to smooth and extend the impulse response function (compare [6, Figs. 7 and 11]). Finally, the simulation current begins at zero whereas the analytical current does not. The flat initial portion of the analytical impulse response function is a result of the assumption of delta-function photon absorption at the p^+ boundary of the device (see Fig. 1). Photon absorption actually takes place more gradually, introducing a dispersion into the initial carrier injection. The principal consequence of this effect, which can be readily calculated, is to remove the flatness from the initial portion of the analytical impulse response function shown in Fig. 8(b). Furthermore, various kinds of specially designed absorption regions can be introduced prior to the MQW device to optimize absorption. This would permit greater multiplication to take place in the device, but at the expense of a decrease in the time-bandwidth product.

The simulation and analytical electron-current contributions to the impulse response function, together with their one-standard-deviation (SD) limits, are shown in Fig. 9(a) and (b), respectively. The simulation 1-SD limits were obtained by repeated computer runs, each using a small number of electrons. The analytical 1-SD limits, on the other hand, were obtained from (9) and (10) or, equivalently, on the basis of formulas for the mean and variance of the gain random variable at each stage [3], [6]. Uncertainty can arise from both gain randomness and transit-time randomness in the physical device, and this is clearly reflected in the uncertain height and uncertain width of the simulation results presented in Fig. 9(a). Only the former source of randomness, however, is permitted within the confines of the deterministic transit-time analytical model.

V. Impulse Response Function for the MQW SAPD Under SCIDCM Conditions

All of the results for the MQW SAPD presented to this point pertain to structures that exhibit only single-carrier-initiated *single*-carrier multiplication (SCISCM). Using the simulation technique, we are able to obtain the im-

pulse response function under single-carrier-initiated *double*-carrier-multiplication (SCIDCM) conditions.

Previous work [12], [14] indicates that significant hole multiplication occurs in GaAs/AlGaAs simple multiquantum-well structures operated at sufficiently high reverse bias to be useful. Therefore, it is necessary to further investigate the temporal response of these devices in the presence of secondary hole ionization. The analytical theory has not yet been extended to the double-carrier multiplication case. However, the numerical model can be used.

The numerical simulation completely tracks all of the carriers, electrons, and holes born during the passage of the initial electron pulse through the device. As described in Section II, an iterative solution is employed. The first electron iteration includes the dynamics of the parent photogenerated electrons and all of the subsequent secondary electrons born from the parents or their direct "descendents." The time and spatial location of the secondary holes born in the first electron iteration are recorded and later simulated in the first hole iteration. In Section IV, we repeated the hole flights in the absence of further carrier multiplication. The response terminated once all of the carriers, electrons, and secondary holes were collected. In the calculations presented below, hole multiplication is included. Therefore, multiple iterations are necessary in order to determine the temporal response. As shown below, the solution converges after three iterations. Therefore, all of the SCIDCM calculations treated here are taken to three iterations.

The instantaneous electron and hole currents, as a function of elapsed time, for the first three iterations are presented in Figs. 10 and 11, respectively, for a five-stage GaAs/AlGaAs simple multiquantum-well APD operated at a reverse-bias field of 350 kV/cm. The lower field used in this case is necessary to avoid avalanche breakdown conditions. The apparent "noisiness" of the hole current is in part due to the choice of scale in the figure. Notice that the hole response lags and extends the electron response significantly; for the first iteration, the hole response (Fig. 11) requires more than 12 ps to decay, roughly twice that for the electrons (Fig. 10).

The overall impulse response function, which is the sum of the electron and hole currents, is presented in Fig. 12. There is a significant difference between the first and third iterations; the duration is increased by ≈ 8 ps. The presence of only a relatively small amount of secondary hole ionization acts to greatly extend the duration of the pulse. In the case presented in Fig. 12, the hole ionization probability is 0.035 per stage while the electron ionization probability is 0.338. Of course, the second and third iterations arise only because of the secondary hole ionization. In its absence, the pulse decays in a much shorter time as illustrated in Fig. 8.

At lower applied fields, where the hole ionization rate is lower, the pulse delay is correspondingly shorter. At sufficiently high applied fields, avalanche breakdown occurs and the impulse response function will not decay at all. This is an unstable operating condition of the device. The applied field of 350 kV/cm chosen here is used as a means of illustrating the temporal response of the device and is not to be considered as the optimal operating point

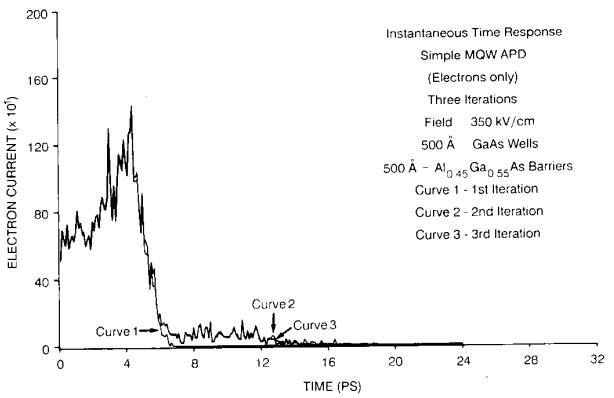

Fig. 10. Electron-current contributions to the impulse response function calculated using the simulation technique in the presence of secondary-hole-initiated ionization events.

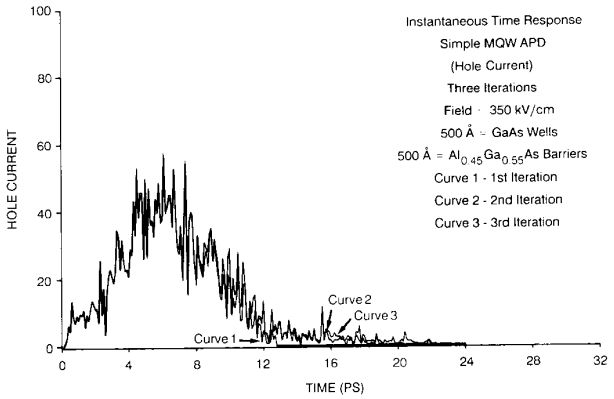

Fig. 11. Hole-current contributions to the impulse response function calculated using the simulation technique under single-carrier-initiated double-carrier-multiplication (SCIDCM) conditions.

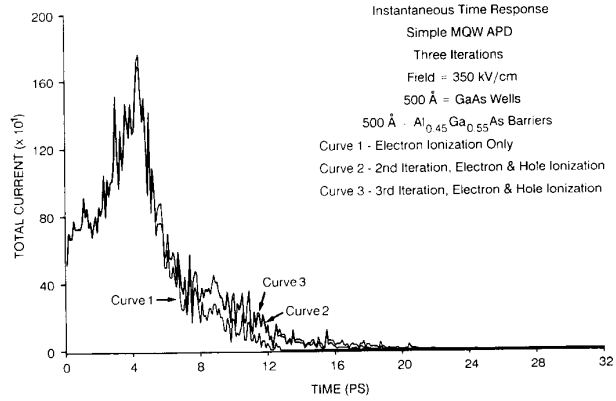

Fig. 12. Overall impulse response function calculated using the simulation technique under SCIDCM conditions. The presence of only a relatively small amount of secondary hole ionization ($Q = 0.035$) acts to greatly extend the duration of the pulse.

of the simple multiquantum well device. Future work will investigate the temporal response of other devices, such as the doped quantum well structures, whose performance is expected to be superior to that of the simple multiquantum-well APD's.

VI. Discussion and Conclusion

The impulse response function for an MQW SAPD was obtained from simulation studies based on electron and hole transport in the device, via an ensemble Monte Carlo approach. The trajectories of a collection of carriers in the device structure were simulated, subject to an applied electric field in conjunction with the device potential profile. The carrier histories were traced in both real space and k-space and the full details of the conduction and valence-band structures and all of the relevant phonon scattering mechanisms have been included. Results were obtained both in the absence of, and in the presence of, hole-initiated impact ionizations. The simulation results in the absence of such events were found to accord reasonably well with calculations based on an analytical model.

The analytical expression for the time course of the impulse response function arising from a single photocarrier entering the multiplication region of an MQW SAPD was derived under the assumption of SCISCM. The model comprises 1) constant (but different) velocities for each carrier in each material and 2) Bernoulli multiplication at each stage of the device. Mathematically, the impulse response function can be described as resulting from a marked filtered Bernoulli branching process [6], where the (deterministic) filter-function shape depends on the stage of initiation, the number of stages of the device, and the mean electron and hole transport times in the two materials. Delta-function absorption was assumed at the p^+ boundary of the multiplication region. The avalanche buildup time τ_{av} was zero since SCISCM conditions were assumed to prevail [28].

The numerical results, using the ensemble Monte Carlo simulation, indicate that the simple analytical expression for the bandwidth

$$B = 1/m(\tau_e + \tau_h) \tag{12}$$

where m is the number of stages, and τ_e and τ_h are the electron and hole transit times per stage, respectively, is invalid due to significant hole multiplication at high applied electric field strengths. Therefore, the bandwidth of these devices can be very much smaller than that predicted under SCISCM conditions, leading to poor temporal response.

Recently, a new device, the doped quantum-well APD [17]–[21], has been proposed that provides nearly four orders or magnitude enhancement in the electron-to-hole ionization rates ratio. As a consequence, this device can provide significant gain while operating under near-SCISCM conditions. The time response of a typical GaAs/AlGaAs p-i-n doped quantum-well APD is presented in Fig. 13. As can be readily seen from this figure, the first and second iterations of the current are essentially

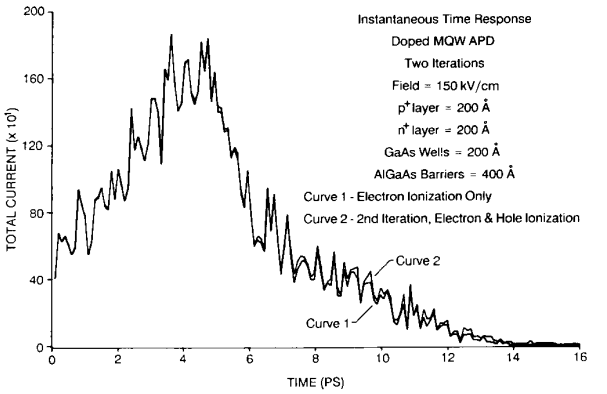

Fig. 13. Overall impulse response function for the doped quantum well device calculated using the simulation technique. Notice that the presence of a vanishingly small hole ionization rate has little effect on the overall time response as indicated by the virtually identical curves for the two iterations.

identical. This implies that the secondary hole ionization, owing to its vanishingly small magnitude, has virtually no effect on the time response of the device. Therefore, the simple bandwidth relation is valid for the doped quantum-well device leading to very high speed performance. The overall applied field used in the simulation is 150 kV/cm, which yields an electron impact ionization probability of 0.332. Future work will investigate in more detail the temporal response of the doped quantum-well structures.

The time response of an APD depends not only upon the avalanche buildup time, but also on the carrier diffusion time and the device RC time constant. These quantities, though important in assessing overall device performance, are less controllable in the design of APD's than the avalanche buildup time. Both the RC time constant and carrier diffusion delay will be roughly the same in comparable APD's since they depend upon parameters that cannot, in general, be further engineered.

An additional factor influencing the temporal response of a multiquantum-well APD is carrier pile-up at the heterobarriers. This effect, present in superlattice/multiquantum well structures, can greatly decrease the bandwidth of the device. In material systems in which the conduction band edge discontinuity is large and the applied electric field is relatively low, extensive trapping of charge carriers within the wells can occur [35]. This in turn leads to very slow device response. We have found [14], [35] that carrier trapping is of greatest importance in the GaInAs/AlInAs system since the conduction band edge is significantly larger, ~ 0.55 eV, and the applied fields necessary to induce impact ionization are much lower than in the GaAs/AlGaAs system. Generally, carrier trapping within GaAs/AlGaAs simple multiquantum well structures does not occur until the applied field becomes less than ~ 150 kV/cm. At this low an applied field, the ionization rate is too low for effective device operation.

In summary, we have presented the basic physics of the temporal response of multiquantum-well APD's using

both analytical and numerical models. It is found that the doped quantum-well APD can mimic SCISCM conditions at useful gain, while the simple MQW APD exhibits a much longer time response than that predicted on the basis of single-carrier-multiplication conditions. Therefore, for high-speed high-gain low-noise operation, the doped quantum-well APD is predicted to well outperform the simple MQW APD.

Acknowledgment

We would like to thank P. Knight and D. Fouts at the Georgia Institute of Technology for technical assistance in the preparation of this manuscript.

References

[1] A. S. Tager, "Current fluctuations in a semiconductor (dielectric) under the conditions of impact ionization and avalanche breakdown," *Sov. Phys.—Solid State*, vol. 6, pp. 1919–1925, 1965.

[2] R. J. McIntyre, "Multiplication noise in uniform avalanche diodes," *IEEE Trans. Electron Devices*, vol. ED-13, pp. 164–168, 1966.

[3] M. C. Teich, K. Matsuo, and B. E. A. Saleh, "Excess noise factors for conventional and superlattice avalanche photodiodes and photomultiplier tubes," *IEEE J. Quantum Electron.*, vol. QE-22, pp. 1184–1193, 1986.

[4] G. E. Stillman and C. M. Wolfe, "Avalanche photodiodes," in *Semiconductors and Semimetals*, vol. 12, R. K. Willardson and A. C. Beer, Eds. New York: Academic, 1977, pp. 291–393.

[5] F. Capasso, "Physics of avalanche photodiodes," in *Semiconductors and Semimetals*, vol. 22, part D, R. K. Willardson and A. C. Beer, Eds. New York: Academic, 1985, pp. 1–172.

[6] K. Matsuo, M. C. Teich, and B. E. A. Saleh, "Noise properties and time response of the staircase avalanche photodiode," *IEEE Trans. Electron Devices*, vol. ED-32, pp. 2615–2623, 1985.

[7] R. Chin, N. Holonyak, Jr., G. E. Stillman, J. Y. Tang, and K. Hess, "Impact ionization in multilayered heterojunction structures," *Electron. Lett.*, vol. 16, pp. 467–469, 1980.

[8] F. Capasso, W. T. Tsang, A. L. Hutchinson, and G. F. Williams, "Enhancement of electron impact ionization in a superlattice: A new avalanche photodiode with large ionization rate ratio," *Appl. Phys. Lett.*, vol. 40, pp. 38–40, 1982.

[9] F.-Y. Juang, U. Das, Y. Nashimoto, and P. K. Bhattacharya, "Electron and hole impact ionization coefficients in GaAs-$Al_xGa_{1-x}As$ superlattices," *Appl. Phys. Lett.*, vol. 47, pp. 972–974, 1985.

[10] F. Osaka, T. Mikawa, and O. Wada, "Electron and hole impact ionization rates in $InP/Ga_{0.47}In_{0.53}As$ superlattice," *IEEE J. Quantum Electron.*, vol. QE-22, pp. 1986–1991, 1986.

[11] K. Brennan, T. Wang, and K. Hess, "Theory of electron impact ionization including a potential step: Application to GaAs-AlGaAs," *IEEE Electron Device Lett.*, vol. EDL-6, pp. 199–201, 1985.

[12] K. Brennan, "Theory of electron and hole impact ionization in quantum well and staircase superlattice avalanche photodiode structures," *IEEE Trans. Electron Devices*, vol. ED-32, pp. 2197–2205, 1985.

[13] K. Brennan, K. Hess, and F. Capasso, "Physics of the enhancement of impact ionization in multiquantum well structures," *Appl. Phys. Lett.*, vol. 50, pp. 1897–1899, 1987.

[14] K. Brennan and Y. Wang, "Field and spatial geometry dependencies of the electron and hole ionization rates in GaAs/AlGaAs multiquantum well APDs," *IEEE Trans. Electron Devices*, vol. ED-35, pp. 634–641, 1988.

[15] G. F. Williams, F. Capasso, and W. T. Tsang, "The graded bandgap multilayer avalanche photodiode: A new low-noise detector," *IEEE Electron Device Lett.*, vol. EDL-3, pp. 71–73, 1982.

[16] F. Capasso, W. T. Tsang, and G. F. Williams, "Staircase solid-state photomultipliers and avalanche photodiodes with enhanced ionization rates ratio," *IEEE Trans. Electron Devices*, vol. ED-30, pp. 381–390, 1983.

[17] H. Blauvelt, S. Margalit, and A. Yariv, "Single-carrier-type dominated impact ionization in multilayered structures," *Electron Lett.*, vol. 18, pp. 375–376, 1982.

[18] K. Brennan, "Theory of the doped quantum well superlattice APD: A new solid state photomultiplier," *IEEE J. Quantum Electron.*, vol. QE-22, pp. 1999–2016, 1986.

[19] ——, "Theory of the GaInAs/AlInAs doped quantum well APD: A new low-noise solid-state photodetector for lightwave communications systems," *IEEE Trans. Electron Devices*, vol. ED-33, pp. 1683–1695, 1986.

[20] ——, "The p-n junction quantum well avalanche photodiode: A new solid state photodetector for lightwave communications systems and on-chip detector applications," *IEEE Trans. Electron Devices*, vol. ED-34, pp. 782–792, 1987.

[21] ——, "The p-n heterojunction quantum well APD: A new high-gain low-noise high-speed photodetector suitable for lightwave communications and digital applications," *IEEE Trans. Electron Devices*, vol. ED-34, pp. 793–803, 1987.

[22] J. S. Smith, L. C. Chiu, S. Margalit, A. Yariv, and A. Y. Cho, "A new infrared detector using electron emission from multiple quantum wells," *J. Vac. Sci. Technol. B*, vol. 1, pp. 376–378, 1983.

[23] S. L. Chuang and K. Hess, "Impact ionization across the conduction-band-edge discontinuity of quantum-well heterostructures," *J. Appl. Phys.*, vol. 59, pp. 2885–2894, 1986.

[24] F. Capasso, J. Allam, A. Y. Cho, K. Mohammed, R. J. Malik, A. L. Hutchinson, and D. Sivco, "New avalanche multiplication phenomena in quantum well superlattices: Evidence of impact ionization across the band-edge discontinuity," *Appl. Phys. Lett.*, vol. 48, pp. 1294–1296, 1986.

[25] K. F. Brennan and C. J. Summers, "The variably spaced superlattice energy filter quantum well avalanche photodiode: A solid state photomultiplier," *IEEE J. Quantum Electron.*, vol. QE-23, pp. 320–327, 1987.

[26] C. J. Summers and K. F. Brennan, "The variably spaced superlattice energy filter, a new device design concept for high energy electron injection," *Appl. Phys. Lett.*, vol. 48, pp. 806–808, 1986.

[27] J. C. Campbell, "High gain-bandwidth product avalanche photodiodes for multigigabit data rate," presented at the Opt. Soc. Amer. Annual Meeting, Seattle, WA, 1986.

[28] M. C. Teich, K. Matsuo, and B. E. A. Saleh, "Time and frequency response of the conventional avalanche photodiode," *IEEE Trans. Electron Devices*, vol. ED-33, pp. 1511–1517, 1986.

[29] S. C. Personick, *Fiber Optics*. New York: Plenum, 1985.

[30] M. C. Teich, K. Matsuo, and B. E. A. Saleh, "Counting distributions and error probabilities for optical receivers incorporating superlattice avalanche photodiodes," *IEEE Trans. Electron Devices*, vol. ED-33, pp. 1475–1488, 1986.

[31] R. B. Emmons and G. Lucovsky, "The frequency response of avalanching photodiodes," *IEEE Trans. Electron Devices*, vol. ED-13, pp. 297–305, 1966.

[32] T. Kaneda, H. Takanashi, H. Matsumoto, and T. Yamaoka, "Avalanche buildup time of silicon reach-through photodiodes," *J. Appl. Phys.*, vol. 47, pp. 4960–4963, 1976.

[33] A. A. R. Riad and R. E. Hayes, "Simulation studies in both the frequency and time domains of InGaAsP-InP avalanche photodetectors," *IEEE Trans. Electron Devices*, vol. ED-27, pp. 1000–1003, 1980.

[34] K. Brennan, "Optimization and modeling of avalanche photodiode structures: Application to a new class of superlattice photodetectors, the p-i-n, p-n homojunction, and p-n heterojunction APDs," *IEEE Trans. Electron Devices*, vol. ED-34, pp. 1658–1669, 1987.

[35] ——, "Theoretical study of multiquantum well avalanche photodiodes made from the GaInAs/AlInAs material system," *IEEE Trans. Electron Devices*, vol. ED-33, pp. 1502–1510, 1986.

*

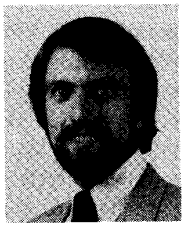

Kevin F. Brennan (S'84–M'84) was born in Elizabeth, NJ, on October 18, 1956. He received the B.S. degree in physics from the Massachusetts Institute of Technology, Cambridge, in 1978, and the M.S. degree in physics and the Ph.D. degree in electrical engineering from the University of Illinois at Urbana-Champaign in 1984.

He is currently an Assistant Professor of Electrical Engineering at the Georgia Institute of Technology. His current research interests include modeling of avalanche photodiodes, high-field effects in compound semiconductors, and transport in submicrometer Si and GaAs devices.

Yang Wang was born in Shanghai, China, on October 29, 1961. He received the B.S.E.E. degree from Shanghai Jiao Tong University, Shanghai, in 1984 and the M.S.E.E. degree from the Georgia Institute of Technology, Atlanta, in 1986. He is currently working toward the Ph.D. degree at the School of Electrical Engineering at Georgia Tech. His research interests concern high-field high-energy transport physics in compound semiconductors and semiconductor devices.

*

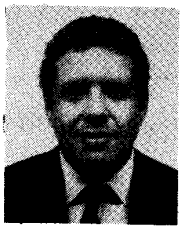

Malvin C. Teich (S'62-M'66-M'72) was born in New York, NY. He received the S.B. degree in physics from the Massachusetts Institute of Technology, Cambridge, in 1961, the M.S. degree in electrical engineering from Stanford University, Stanford, CA, in 1962, and the Ph.D. degree in quantum electronics from Cornell University, Ithaca, NY, in 1966.

In 1966 he joined the MIT Lincoln Laboratory, Lexington, MA, where he was engaged in work on coherent infrared detection. In 1967, he became a member of the faculty in the Department of Electrical Engineering, Columbia University, New York, NY, where he is now teaching and pursuing his research interests in the areas of optical and infrared detection, quantum optics, lightwave communications, and sensory perception. He served as Chairman of the Department from 1978 to 1980. He is also a member of the faculty in the Department of Applied Physics and Nuclear Engineering, and a member of the Columbia Radiation Laboratory, the Center for Telecommunications Research, and the Columbia Bioengineering Institute. He has authored or coauthored some 100 technical publications and holds one patent.

Dr. Teich is a member of Sigma Xi, the American Physical Society, the Acoustical Society of America, the Society for Neuroscience, the American Association for the Advancement of Science, and the New York Academy of Sciences. He served as a member of the Editorial Advisory Panel for *Optics Letters* from 1977 to 1979. In 1969 he was the recipient of the IEEE Browder J. Thompson Memorial Prize for his paper "Infrared Heterodyne Detection" and in 1981 he received the Citation Classic Award of *Current Contents* for this work. He was appointed a Fellow of the John Simon Giggenheim Memorial Foundation in 1973 and was elected a Fellow of the Optical Society of America in 1983.

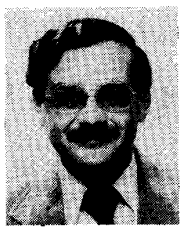

Bahaa E. A. Saleh (M'73-SM'86) received the B.S. degree from Cairo University in 1966 and the Ph.D. degree from the Johns Hopkins University in 1971, both in electrical engineering.

From 1971 to 1974 he was an Assistant Professor at the University of Santa Catarina, Brazil. Thereafter, he joined the Max Planck Institute in Göttingen, Germany, where he was involved in research in laser light scattering and photon correlation spectroscopy. He is presently Professor of Electrical and Computer Engineering at the University of Wisconsin, Madison, where he has been since 1977. He held visiting appointments at the University of California, Berkeley, in 1977, and the Columbia Radiation Laboratory of Columbia University in 1983. He is currently involved in research in image processing, optical information processing, statistical optics, optical communication, and vision. He is the author of *Photoelectron Statistics* (Springer, 1987) and a co-editor of *Transformations in Optical Signal Processing* (SPIE, 1981). In 1980-1983 he was an associate editor of the *Journal of the Optical Society of America*, and since 1983 he has been a topical editor of the same journal.

Dr. Saleh is a Fellow of the Optical Society of America and a member of Phi Beta Kappa and Sigma Xi. He was appointed a Fellow of the John Simon Guggenheim Foundation in 1984.

*

Toofan Khorsandi was born in Tehran, Iran, on August 27, 1964. He received the B.S. degree in computer and electronics engineering in 1986 from George Mason University, Fairfax, VA, and the M.S. degree in electrical engineering in 1988 from Columbia University, New York City, where he was engaged in research on analytical modeling of optoelectronic devices at the Center for Telecommunications Research.

He is currently employed at HHB Systems, Mahwah, NJ, as a member of the CAE Software Development Group.